



Recent development of two-dimensional transition metal dichalcogenides and their applications

Wonbong Choi^{1,*}, Nitin Choudhary¹, Gang Hee Han^{2,3}, Juhong Park¹, Deji Akinwande⁴ and Young Hee Lee^{2,3,*}

¹ Department of Materials Science and Engineering, Mechanical and Energy Engineering, University of North Texas, Denton, TX 76207, United States

² Center for Integrated Nanostructure Physics, Institute for Basic Science (IBS), Suwon 16419, Republic of Korea

³ Department of Energy Science, Sungkyunkwan University (SKKU), Suwon 16419, Republic of Korea

⁴ Department of Electrical and Computer Engineering, The University of Texas at Austin, Austin, TX 78758, United States

Recent advances in atomically thin two-dimensional transition metal dichalcogenides (2D TMDs) have led to a variety of promising technologies for nanoelectronics, photonics, sensing, energy storage, and opto-electronics, to name a few. This article reviews the recent progress in 2D materials beyond graphene and includes mainly transition metal dichalcogenides (TMDs) (e.g. MoS₂, WS₂, MoSe₂, and WSe₂). These materials are finding niche applications for next-generation electronics and optoelectronics devices relying on ultimate atomic thicknesses. Albeit several challenges in developing scalable and defect-free TMDs on desired substrates, new growth techniques compatible with traditional and unconventional substrates have been developed to meet the ever-increasing demand of high quality and controllability for practical applications. The fabrication of novel 2D TMDs that exhibit exotic functionalities and fundamentally new chemistry is highlighted. And finally, in parallel with the electronics, the considerable effort devoted to using these materials for energy and sensing applications is discussed in detail.

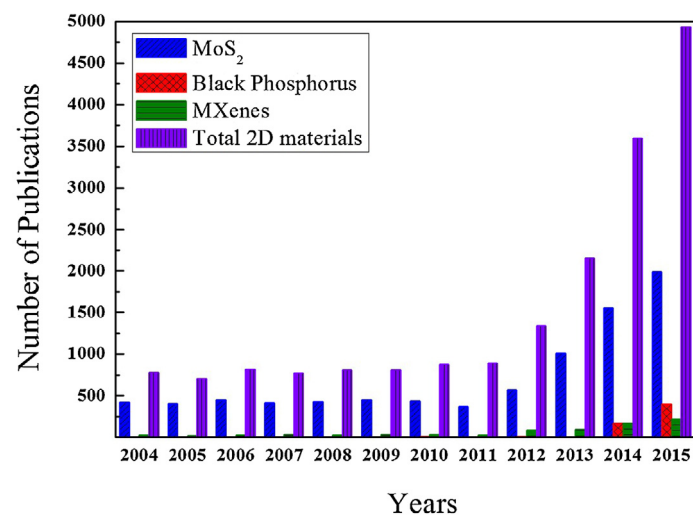
Introduction

The great success of graphene has been followed by an equally impressive surge for the development of other 2D materials that can form atomic sheets with extraordinary properties. Interestingly, the 2D library grows every year and feature more than 150 exotic layered materials that can be easily split into a subnanometer-thick materials [1–3]. These include 2D TMDs (e.g. molybdenum disulfide (MoS₂), molybdenum diselenide (MoSe₂), tungsten disulfide (WS₂), and tungsten diselenide (WSe₂)), hexagonal boron nitride (h-BN), borophene (2D boron), silicene (2D silicon), germanene (2D germanium), and MXenes (2D carbides/nitrides) [4–11]. Figure 1 is a year-wise publication list of 2D materials that show the increasing trend of studying TMDs. Depending on their chemical compositions and structural configurations, atomically thin 2D materials can be categorized as metallic, semi-metallic,

semiconducting, insulating, or superconducting. The first graphene descendants that sparked intense research activity are TMDs, which are almost as thin, transparent and flexible as graphene [12,13]. Unlike graphene, many 2D TMDs are semiconductor in nature and possess huge potential to be made into ultra-small and low power transistors that are more efficient than state-of-the-art silicon based transistors fighting to cope with ever-shrinking devices [14,15]. Besides sharing the similarities of a band gap in the visible-near IR range, high carrier mobility, and on/off ratio with ubiquitous silicon, TMDs can be deposited onto flexible substrates and survive the stress and strain compliance of flexible supports [16,17].

2D TMDs exhibit unique electrical and optical properties that evolve from the quantum confinement and surface effects that arise during the transition of an indirect bandgap to a direct bandgap when bulk materials are scaled down to monolayers. This tunable bandgap in TMDs is accompanied by a strong photoluminescence

*Corresponding authors: Choi, W. (wonbong.choi@unt.edu), Lee, Y.H. (leeyoung@skku.edu)

**FIGURE 1**

Year-wise publication plots for 2D TMDs including MoS₂, MoSe₂, black phosphorus, MXenes, and total 2D TMDs in the period of 2005–2016 (searched by SciFinder Scholar (<https://scifinder.cas.org>), American Chemical Society database (<https://www.acs.org/content/acs/en.html>), August 10th, 2016).

(PL) and large exciton binding energy, making them promising candidate for a variety of opto-electronic devices, including solar cells, photo-detectors, light-emitting diodes, and photo-transistors [18–22]. For example, unique properties of MoS₂ include direct bandgap (~1.8 eV), good mobility (~700 cm² V⁻¹ s⁻¹), high current on/off ratio of ~10⁷–10⁸, large optical absorption (~10⁷ m⁻¹ in the visible range) and a giant PL arising from the direct bandgap (1.8 eV) in monolayer; thus, it has been studied widely for electronics and optoelectronics applications [23].

van der Waals (vdW) gaps between each neighboring layer and large specific surface area due to sheet-like structures are distinct features that make 2D TMDs highly attractive for capacitive energy storage (e.g. supercapacitors and batteries) and sensing applications [24,25]. The large surface-to-volume ratio bestows 2D TMDs based sensors with improved sensitivity, selectivity and low power consumption. Unlike digital sensors, TMDs based sensors do not have physical gates for selectively reacting to the targeted gas molecules or biomolecules [26,27]. MoS₂-based FET devices have potential applications in gas, chemical, and bio-sensors. Another aspect of the weakly bonded 2D TMDs atomic layers is that they can be easily isolated and stacked with other TMDs to construct a wide range of vdW heterostructures without the limitation of lattice matching [28,29]. Stacking together one-atom-thick sheets of dissimilar TMDs, for example, vertically stacked heterostructures allows for the realization of unique functions and superior properties that cannot be obtained otherwise. By exploiting such novel properties in these vdW heterostructures as band alignment, tunneling transports, and strong interlayer coupling, several new electronic/opto-electronic devices such as tunneling transistors, barristers, photodetectors, LEDs and flexible electronics can be fabricated [30,31]. Figure 2 depicts the diverse devices constructed from the 2D TMDs by using their unique physical, chemical, and opto-electronic properties [32–37].

Even though 2D TMDs exhibit a breadth of new properties that are distinct from traditional bulk materials or thin films,

developing such materials into large-scale and defect-free atomic layers with thickness controllability on desired substrates is challenging. The state-of-art mechanical exfoliation method produces high quality monolayers of TMDs, but this technique is not scalable [38,39]. Chemical vapor deposition (CVD) is one possible way of doing this due to its potential for high scalability and degree of morphological control [40]. Recent developments have led to marked improvements in the quality of TMD layers produced via CVD method. Metal-organic CVD (MOCVD) and atomic layer deposition (ALD) are the other emerging candidates for the growth of wafer-scale and highly quality TMD films [41,42]. TMDs grown by these methods are not only uniform over the entire substrate, but also are comparable in performance to the atomic layers produced by the standard exfoliation method.

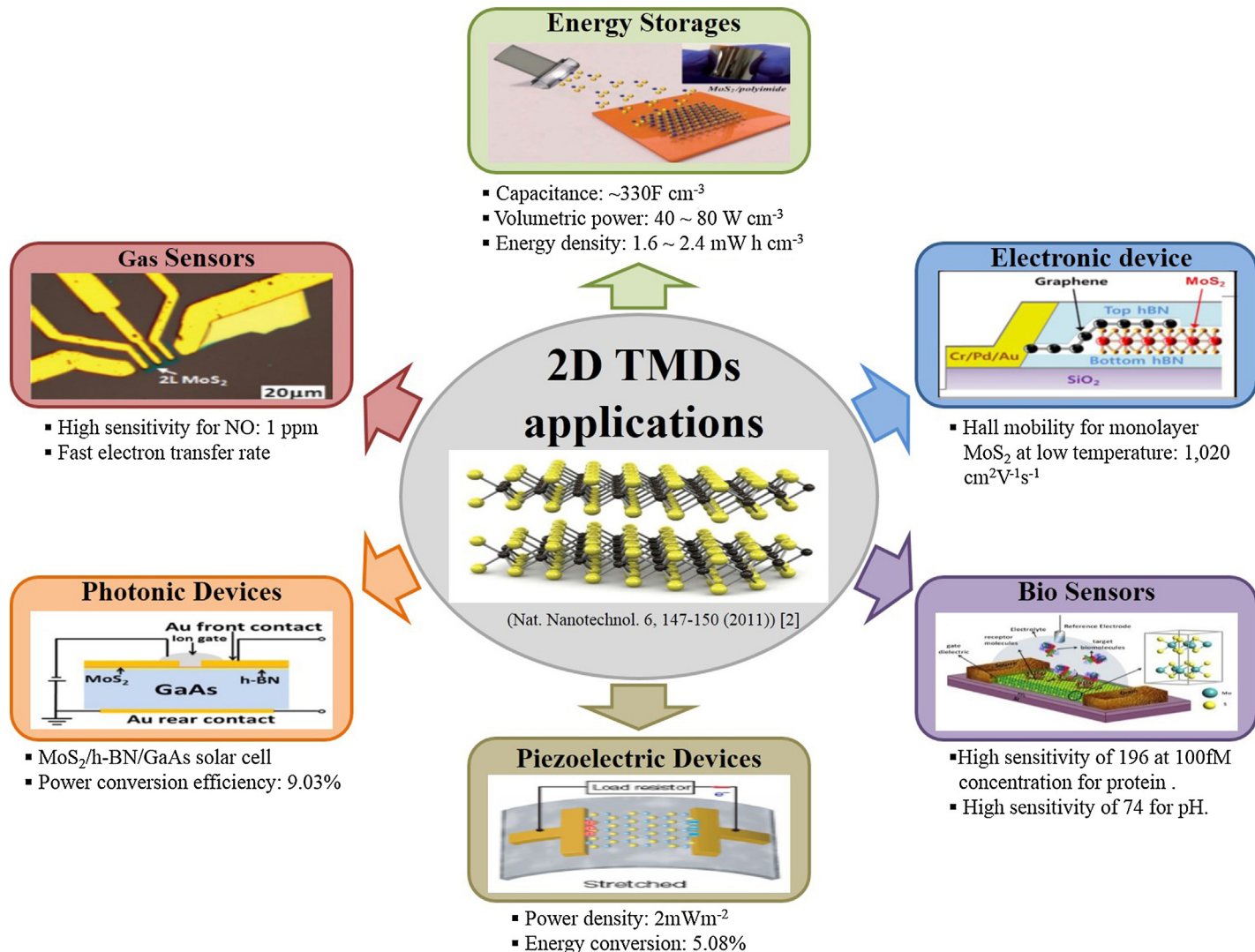
The field of 2D materials is an ever-expanding research area, and the search for other 2D materials beyond graphene is not just limited to TMDs. New 2D materials such as silicene and phosphorene are strong contenders in the rapidly emerging realms of 2D materials [43,44]. Several theoretical studies address the fundamental properties of these new 2D materials; however, experimental perspectives are still in their infancy due to stability issues.

This review highlights the recent advances in the synthesis of large-scale and defect-free 2D TMDs. Moreover, we focus on the recent progress in electronic, opto-electronic, and electrochemical properties of newly studied TMDs with rational designs and new structures for potential applications in electronics, sensors, and energy storages. Additionally, we discuss recent breakthroughs in the newest families of 2D materials like silicene and phosphorene. The wide range of interesting properties and potential for use in emergent technologies suggest TMDs are likely to remain an important research area for years to come.

Crystal structure and physical properties

TMDs are layered materials in which each unit (MX₂) is composed of a transition metal (M) layer sandwiched between two chalcogen (X) atomic layers. Depending on the arrangement of the atoms, the structures of 2D TMDs can be categorized as trigonal prismatic (hexagonal, H), octahedral (tetragonal, T) and their distorted phase (T') as shown in Fig. 3a. Typical atomic ratio in layered TMDs exhibits one transition metal to two chalcogen atoms to create MX₂ except several cases such as 2:3 quintuple layers (M₂X₃) [45] and 1:1 metal chalcogenides (MX) [46]. In H-phase material, each metal atom puts six branches out to two tetrahedrons in +z and -z directions while the hexagonal symmetry can be seen in the top view (Fig. 3a). Therefore, chalcogen–metal–chalcogen arrangement along z-direction is considered as single layer, and weak vdW interactions between each layer (chalcogen–chalcogen) enable mechanical exfoliation from bulk TMDs to obtain single layer flake. T-phase has a trigonal chalcogen layer on the top and 180 degree rotated structure (so-called trigonal antiprism) at the bottom in a single layer and results in hexagonal arrangement of chalcogen atoms in the top view. Metal atoms are distorted further (or dimerized in one direction), called T'-phase [47,48], resulting in the modification of atomic displacement of chalcogen atoms along z-direction (8).

Despite the extraordinary mobility of electrons (i.e. ~15,000 cm² V⁻¹ s⁻¹ at room temperature) in graphene, the lack of a bandgap restricts its use as an active element in FETs [49].

**FIGURE 2**

Electronic, opto-electronic and energy devices based on 2D transition metal dichalcogenides (TMDs). (Reprinted with permission from Ref. [32]. 2015, Nature Publishing Group; Ref. [33]. 2014, Nature Publishing Group; Ref. [34]. 2015, Royal Society of Chemistry; Ref. [35]. 2012, John Wiley and Sons; Ref. [36]. 2015, Nature Publishing Group; and Ref. [37]. 2014, American Chemical Society.)

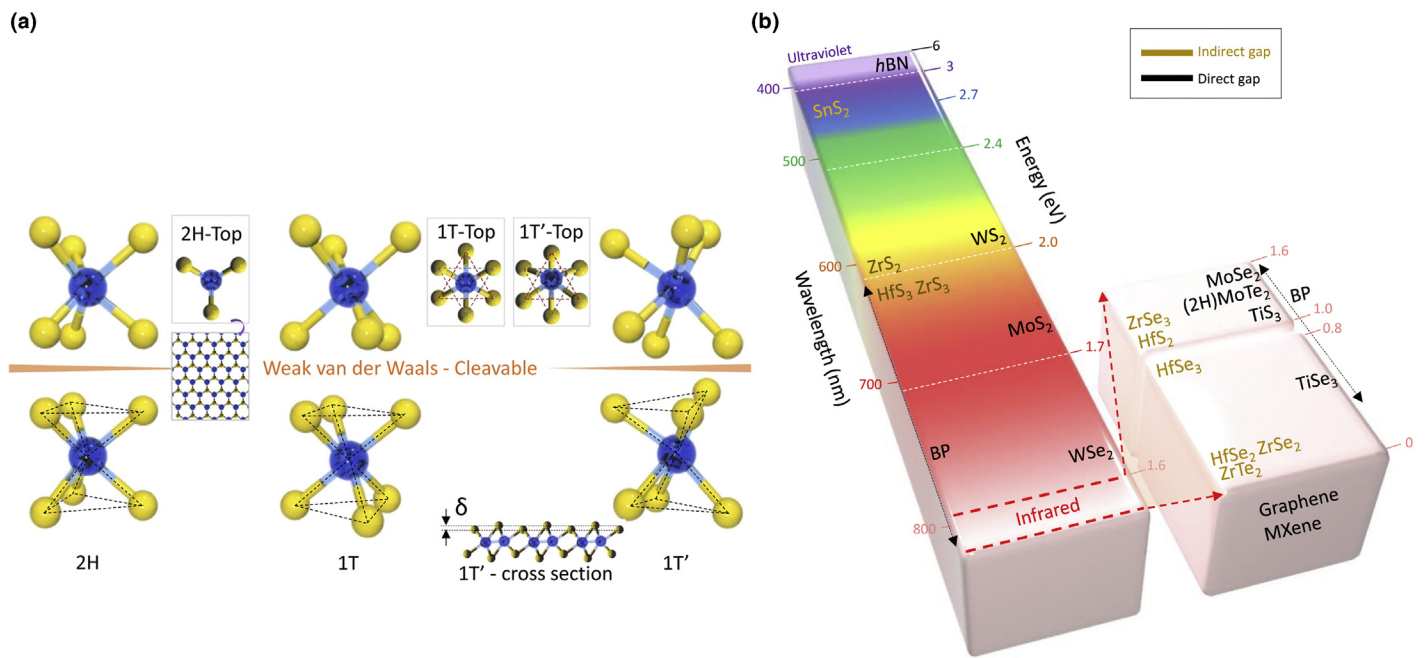
Tremendous efforts to open the bandgap of graphene using nanoribbons, AB-stacked bilayer graphene, and chemical doping have met with marginal success providing the bandgap opening up to 200 meV in most cases [50–52].

This remains a challenging issue and has been a driving force in developing 2D TMDs with a finite bandgap. As listed in Fig. 3b, 2D TMDs reveal a wide range of bandgap covering all visible and infrared range with the choice of material [53]. Most semiconducting 2D TMDs reveal direct bandgap in monolayer, whereas they are indirect bandgap in bulk form except few cases of GaSe and ReS₂ [54,55]. For example, monolayer dichalcogenides such as MoS₂ (1.8 eV), MoSe₂ (1.5 eV), (2H)-MoTe₂ (1.1 eV), WS₂ (2.1 eV) and WSe₂ (1.7 eV) show direct bandgap, whereas bulk phases exhibit indirect gap with smaller energies. Most MX₂ materials have both metallic phase and semiconducting phase [56]. The stable phase of MX₂ material at room temperature is 2H phase, whereas 1T phase can be obtained by Li-intercalation [57] or electron beam irradiation [58]. The chemically exfoliated 1T MoS₂ phase is known to be

10⁷ times more conductive than the semiconducting 2H phase [59]. In case of WTe₂, 1T or 1T' phase is more stable than 2H phase at room temperature [60]. Both 2H and 1T' phase in MoTe₂ can be easily modulated into each other because the cohesive energy difference between both phases is similar to each other. Besides, the dichalcogenides of titanium (Ti), chromium (Cr), nickel (Ni), zinc (Zn), vanadium (V), niobium (Nb), and tantalum (Ta) simply exhibit metallic behavior [61].

Since most of the MX₂ are free from dangling bonds, and some of them exhibit high mobility, depending on the choice of appropriate substrate and metal contacts as well as mobility suppression through grain boundaries, etc. For example, MoS₂ gives a mobility of 700 cm² V⁻¹ s⁻¹ on SiO₂/Si substrate with scandium (Sc) contact and 33–151 cm² V⁻¹ s⁻¹ on BN/Si substrate (encapsulated) at room temperature [62,63].

Besides excellent electrical transport, TMDs are mechanically flexible and strong similar to graphene. An exceptionally high Young's modulus (E) of $\sim 0.33 \pm 0.07$ TPa has been reported in

**FIGURE 3**

(a) Typical structures of layered transition metal dichalcogenides. Cleavable 2H, 1T and 1T' structures in layered TMD are shown. (b) Bandgap of 2D layered materials varying from zero band gap of graphene (white color) to wide bandgap of hBN. The color in the column is presenting the corresponding wavelength of bandgap, for example, the bandgap for MoS₂ (1.8 eV) is red color and WS₂ (2.0 eV) is orange color. Indirect materials are represented at left (SnS₂, ZrS₂, HfS₃, ZrS₃, ZrSe₃, HfS₂, HfSe₃, HfSe₂, ZrSe₂ and ZrTe₂) and direct bandgap materials are represented at right side of the column (h-BN, WS₂, MoS₂, WSe₂, MoSe₂, 2H-MoTe₂, TiS₃ and TiSe₃).

suspended few-layer MoS₂ nanosheets [64]. Bertolazzi et al. [65] reported high in-plane stiffness and E of single-layer MoS₂, that is, $\sim 180 \pm 60$ N m⁻¹ and $\sim 270 \pm 100$ GPa, respectively. The Young's modulus of monolayer MoS₂ outperforms the stainless steel (204 GPa) and graphene oxide (207 GPa) [66], which are attributed to the absence of stacking faults, high crystallinity and defect-free nature of the atomically thin TMDs.

More recent progress in single component 2D layers is expanded to the group III and V elements. Atomically thin boron layer 'borophene' synthesis was recently carried out in an ultrahigh vacuum system with the evaporation of pure boron element at high temperature (450–700°C) on silver (Ag) (111). Anisotropic metallicity is confirmed by scanning tunneling spectroscopy, while bulk boron allotropes are semiconductors [67]. Bulk black phosphorous (BP) was synthesized by chemical vapor transport of red phosphor in the presence of transport agent [68] or pressurization (>1.2 GPa, 200°C) [69,70]. BP film is a strong candidate for applications to electronic devices due to their high mobility (~ 1000 cm² V⁻¹ S⁻¹) with ambipolarity [71–73]. Layered metal carbides/nitrides, MXenes [74], are located at the bottom in the schematic with graphene also show metallic behavior.

The structure and properties such as charge density wave (CDW), magnetism (ferromagnetic and anti-ferromagnetic), and superconductivity of 2D TMDs are summarized in Fig. 4. The detail description of all these properties in each material is beyond the scope of this review.

In addition to TMDs, borophene, silicene, germanene and stanene are predicted as exotic 2D materials that could show many intriguing properties. However, these materials are quite unstable in air [75] and therefore need encapsulation or

hydrogen termination to generate SiH or GeH in silicene or germanene. Borophene is characterized as a metal. Silicene opens a bandgap slightly by 1.9 meV and germanene by 33 meV and stanene by 101 meV, which is an opposite trend with atomic number [76]. Recent work reveals the performance of silicene as a field effect transistor (FET), which is promising for future

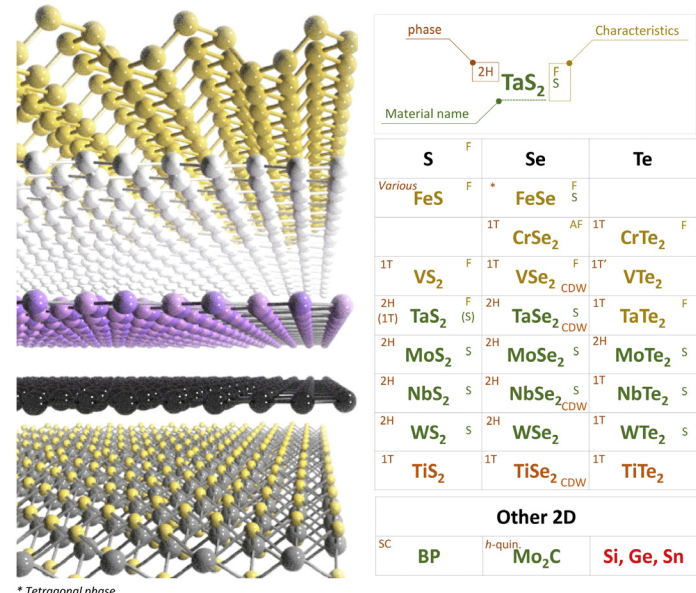
**FIGURE 4**

Table for various 2D TMDs and other 2D materials exhibiting various physical properties such as magnetism (ferromagnetic (F)/anti-ferromagnetic (AF)), superconductivity (s) and charge density wave (CDW) and crystal structures (2H, 1T).

electronics [77]. Stanene is predicted as a candidate of 2D topological layer.

Recent advance in synthesis processes for 2D TMDs

Considerable efforts have been devoted to the synthesis of controllable, large-scale, and uniform atomic layers of diverse 2D TMDs using various top-down and bottom-up approaches, including mechanical exfoliation, chemical exfoliation, and chemical vapor deposition (CVD). Most of the reported data and theory on the fundamental physics and devices on 2D TMDs have largely relied on the exfoliation method due to its high quality. However, the critical limitations of the flake size and film uniformity have dragged its development beyond the fundamental studies. On the contrary, the CVD process has been studied for scalable and reliable production of large area 2D TMDs. Nevertheless, CVD grown TMDs show poor quality as compared to their exfoliated counterparts.

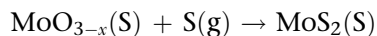
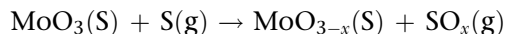
Very recently, attempts have been made to obtain high quality TMDs with thickness controllability and wafer-scale uniformity using atomic layer deposition (ALD), metal-organic-CVD (MOCVD), and direct deposition methods (sputtering, pulsed laser deposition (PLD), e-beam). The 2D materials forming chemical reactions generally use either thermal energy from a heated substrate or non-thermal energy such as microwave or photon energy into the reaction process and the 2D materials forming process depends on lattice parameter of substrates, temperatures, and atomic gas flux [78,79]. Here, we will focus our discussion on the 2D TMDs growth by CVD, MOCVD, and ALD methods with their pros and cons.

Chemical vapor deposition/vapor phase growth process

The CVD is one of the most effective methods to achieve large area growth of atomically thin 2D TMDs for the successful device applications. The simplest form of CVD to grow 2D TMDs is the co-evaporation of metal oxides and chalcogen precursors that lead to vapor phase reaction followed by the formation of a stable 2D TMD over a suitable substrate. The growth mechanism of CVD method differs in each synthesis process as the materials forming process also depends on (1) properties of substrate, (2) temperature and (3) atomic gas flux as briefly discussed in the following section.

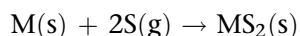
(1) *Properties of substrate*: the atomic layer of 2D materials is influenced by nanoscale surface morphology and terminating atomic planes of substrates as well as lattice mismatching. It was reported that the surface energy of substrate affects the nucleation and growth of 2D TMDs [80]. (2) *Temperature*: the reaction process is limited by the growth temperature. Normally, if the growth temperature is high, that is, the surface diffusion is fast enough, a randomly deposited adatom will move to the energetically most favorable places and results in a 3D island growth. On the other hand, if the substrate temperature is too low, an amorphous or polycrystalline film will form since adatoms will not have enough kinetic energy to diffuse and find the lowest potential energy site [81]. (3) *Atomic gas flux*: atomic gas flux is another important parameter to achieve high quality 2D materials growth. Only a sufficient high vapor pressure enables mixing of atomic gases and transport the atomic species to the substrate. The stability of vaporized atoms is required to prevent unnecessary reaction during vaporized atom transport to the substrate. The

vaporized atoms are transported by a carrier gas to the substrate and the flow rate of vaped atom is governed by the Clausius–Clapeyron equation: $d(\ln P)/dT = \Delta H/kT$, where ΔH is the enthalpy of evaporation, P is the partial pressure of the evaporated atom [82]. Lee et al. [83] reported large-scale MoS₂ layers by chemical vapor reaction of molybdenum trioxide (MoO₃) and sulfur powder at elevated temperatures ($\sim 650^\circ\text{C}$). MoO₃ is initially reduced into a sub oxide MoO_{3-x}, which reacts with vaporized sulfur further to form a 2D layered MoS₂ film.



This simple process is capable of producing large-scale MS₂; however, it often results in the formation of randomly distributed flakes rather than a continuous film. The inhibition of the growth of MoS₂ was attributed to the presence of interfacial oxide layer as a significant obstacle. In a similar approach, Najmaei et al. [84] synthesized MoS₂ atomic layers on Si/SiO₂ substrates by using the vapor-phase reaction of MoO₃ and S powders and reported the formation of MoS₂ monolayer triangular flakes on the substrates rather than the formation of a continuous MoS₂ layer. The average mobility and maximum current on/off ratio of the MoS₂ flakes showed $4.3 \text{ cm}^2 \text{ V}^{-1} \text{ s}^{-1}$ and $\sim 10^6$, respectively. Wang et al. [85] found an interesting shape evolution in CVD grown MoS₂ domains from triangular to hexagonal geometries depending upon the spatial location of the silicon substrate as shown in Fig. 5a. Yu et al. [86] developed a new method that precisely control the number of MoS₂ layers over a large area by using MoCl₅ and sulfur as precursors. But, the mobility of charge carriers in MoS₂-FET was found to be very low ($0.003\text{--}0.03 \text{ cm}^2 \text{ V}^{-1} \text{ s}^{-1}$).

Another facile method for growing large area and continuous TMDs is using the ‘two-step method’, depositing transition metal thin film (e.g. Mo, W, Nb, etc.) on substrate (usually Si/SiO₂) followed by thermal reaction with chalcogen (S, Se, Te) vapor. The following reaction occurs to form a stable 2D TMD during the CVD process at high temperatures ($300\text{--}700^\circ\text{C}$) and inert atmosphere.



This ‘two-step method’ has demonstrated wafer scale fabrication (~ 2 in.) and successful thickness modulation of MoS₂ layers (multilayer to monolayer) on SiO₂/Si substrates (Fig. 5b) [87]. After metal deposition (W, Mo) with controlled thickness, the metal-coated substrate and sulfur powder were placed inside the CVD furnace, and the reaction environment was kept inert under a constant flow of ~ 200 sccm Ar at 600°C for 90 min. However, in monolayer MoS₂ grown, point defects and double layers’ domains were present as confirmed by high-resolution transmission electron microscopy (HRTEM) and Raman analysis. Electrical measurements on MoS₂ FETs revealed a semiconductor behavior with much higher field effect mobility ($\sim 12.24 \text{ cm}^2 \text{ V}^{-1} \text{ s}^{-1}$) and current on/off ratio ($\sim 10^6$) as compared to previously reported CVD-grown MoS₂-FETs and amorphous silicon (a-Si) or organic thin film transistors. Zhan et al. [88] used e-beam evaporation and CVD methods to grow large area MoS₂ films and found a p-type conduction but with very poor mobilities in the range of $0.004\text{--}0.04 \text{ cm}^2 \text{ V}^{-1} \text{ s}^{-1}$. The presence of Mo-containing seeds has been

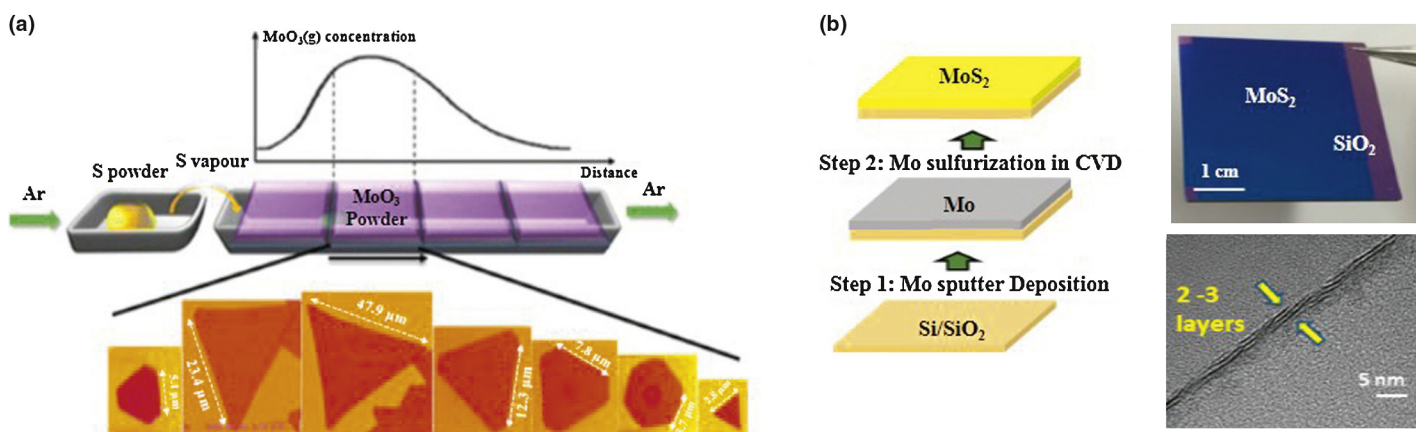


FIGURE 5

(a) Schematic diagram of CVD process and AFM images showing shape evolution of MoS₂ crystals from triangular to hexagonal depending on the spatial location of silicon substrate. (Reprinted with permission from Ref. [85]. 2014, American Chemical Society.) (b) Large area growth of 2–3 layers of MoS₂ using Mo seed layer sulfurized in a CVD furnace. (Reprinted with permission from Ref. [87]. 2015, American Institute of Physics.)

shown to provide predefined location for nucleation and growth of highly crystalline monolayer MoS₂ [89]. The patterns or seed molecules on the substrates can provide the controlled nucleation of 2D TMDs in predefined locations. The growths of large crystalline island of MoS₂ with a size of 100 μm were reported. Device measurements exhibited carrier mobility and on/off ratio that exceeded 10 cm² V⁻¹ s⁻¹ and 10⁶, respectively. However, the metal-sulfurization method offers controllable thickness with large scale production, but it is still limited to the production of small grain size with defects. In addition to metal film approach, direct sulfurization/selenization of various metal oxide and chloride precursors such as (NH₄)₂MoS₄, MoO₃, WO₃ and MoO₂ have been widely employed to grow TMDs. Elias et al. [90] controlled the thickness of the WO₃ coating for the large-area growth of single-layer and few-layer WS₂ sheets. (NH₄)₂MoS₄ and similar sulfide precursors have been used, but with uncontrolled layer thicknesses [91]. During selenization of oxide and chloride coatings, hydrogen gas is usually introduced to assist the reaction and to help in tailoring the crystalline shape of TMDs [92].

Metal-organic chemical vapor deposition (MOCVD)

The MOCVD is similar to a conventional CVD except that metal-organic or organic compound precursor are used as the source materials [93,94]. In MOCVD reaction, the desired atoms are combined with complex organic molecules and flown over a substrate where the molecules are decomposed by heat and the target atoms are deposited on the substrate atom by atom. The quality of films can be engineered by varying the composition of atoms at atomic scale, which results in the desired thin film with high crystallinity. Figure 6 is the representative schematic of the MOCVD method showing various steps involved during the synthesis of 2D materials. As shown in Fig. 6, a series of surface reactions occur during MOCVD process including adsorption of precursor molecules followed by surface kinetics (i.e. surface diffusion), nucleation and growth of desired material with the desorption of the volatile product molecules.

MOCVD has been used to grow 2D TMDs only very recently. The advantages of MOCVD in 2D TMDs growth are: (i) it can achieve large-scale and uniform growth of 2D TMDs, (ii) it provides

a precise control over both metal and chalcogen precursors and thereby controls the composition and morphology of 2D TMDs. In this regard, Kang et al. [95] synthesized wafer-scale (4-in.) monolayer and few layers MoS₂ and WS₂ films on SiO₂ substrates by using molybdenum hexacarbonyl (Mo(CO)₆), tungsten hexacarbonyl (W(CO)₆), ethylene disulfide ((C₂H₅)₂S), and H₂ gas-phase precursors with Ar gas carrier. The team shows large-scale MoS₂ and WS₂ films on 4-in. fused silica substrates (Fig. 7a), and about 8000 MoS₂ FET devices fabricated by a standard photolithography process (Fig. 7b). The MoS₂-FETs showed high electron mobility of ~30 cm² V⁻¹ s⁻¹ at room temperature and 114 cm² V⁻¹ s⁻¹ at 90 K (Fig. 7c). Figure 7d is the time evolution of the monolayer coverage over the entire substrate as a function of critical time (t_0).

Recently, Eichfeld et al. [96] claimed the first report on the large-area growth of mono and few-layer WSe₂ via MOCVD using W(CO)₆ and dimethylselenium ((CH₃)₂Se) precursors. They showed that the temperature, pressure, Se:W ratio, and substrate choice that have significant impact on the morphology of WSe₂ films. It is clear from Fig. 8a that WSe₂ has distinct morphology on different substrates including epitaxial graphene, CVD graphene, sapphire and BN. WSe₂ grew with large nucleation density on

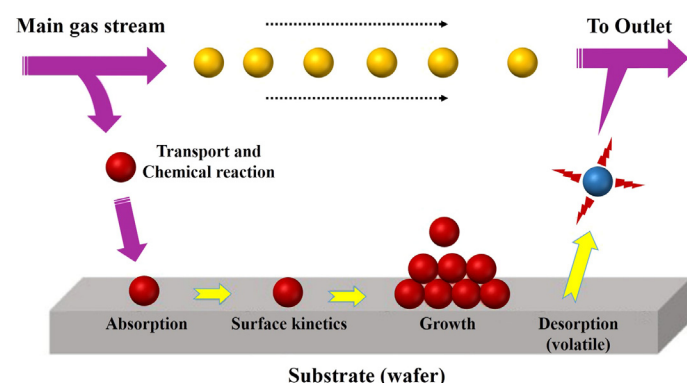


FIGURE 6

Deposition process on the substrate and surface processes in MOCVD while growing active layers on the substrate. The gaseous precursors are thermally decomposed and adsorbed on the substrate followed by surface diffusion kinetics to form high quality thin films.

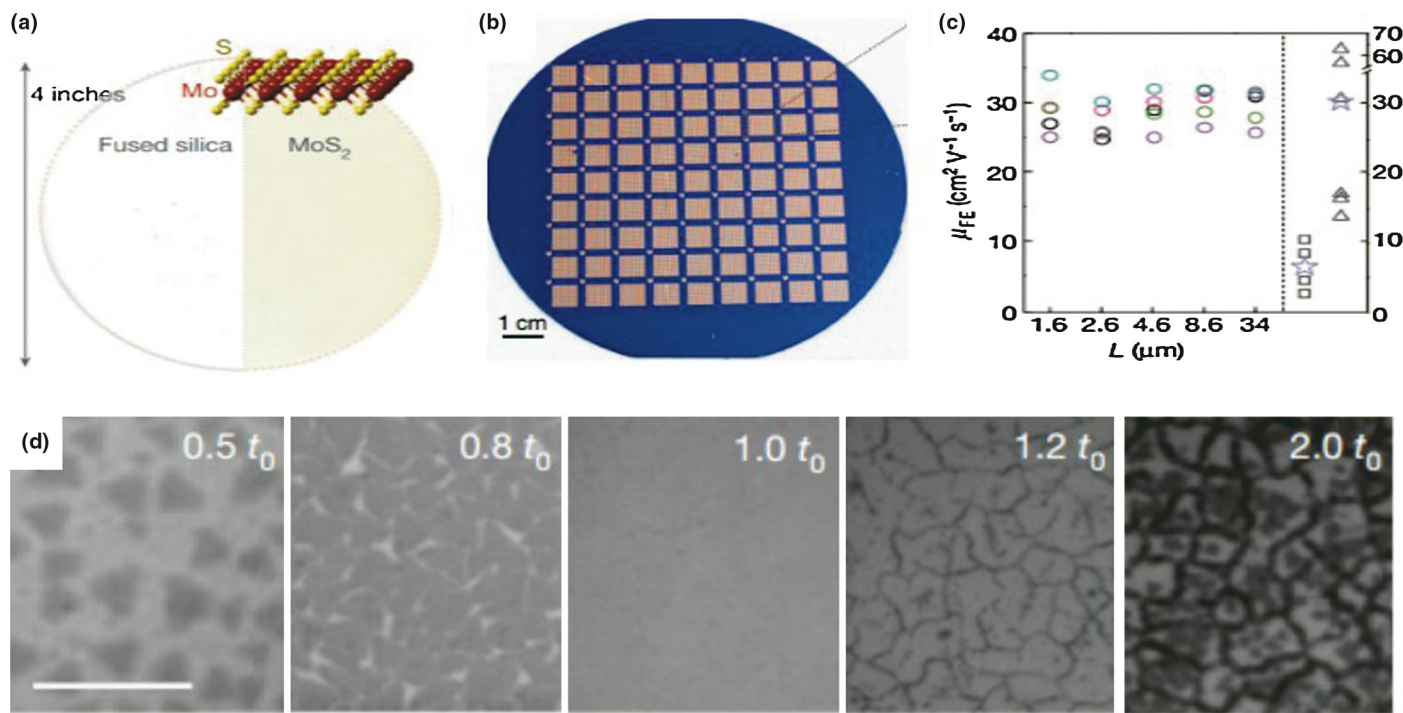


FIGURE 7

Large scale MOCVD growth of continuous (a) MoS₂ monolayers on fused silica using all-gas phase precursors. (b) The scalable growth enables mass production of ~8000 of FET devices. (c) Field effect mobility (μ_{FE}) measured from five FET devices with different length scales. A consistent mobility of $\sim 30 \text{ cm}^2 \text{ V}^{-1} \text{ s}^{-1}$ was observed. (d) Optical images of MoS₂ films at different growth times, where t_0 is the optimal growth time for full monolayer coverage (scale bar: 10 μm). (Reprinted with permission from Ref. [95]. 2015, Nature Publishing Group.)

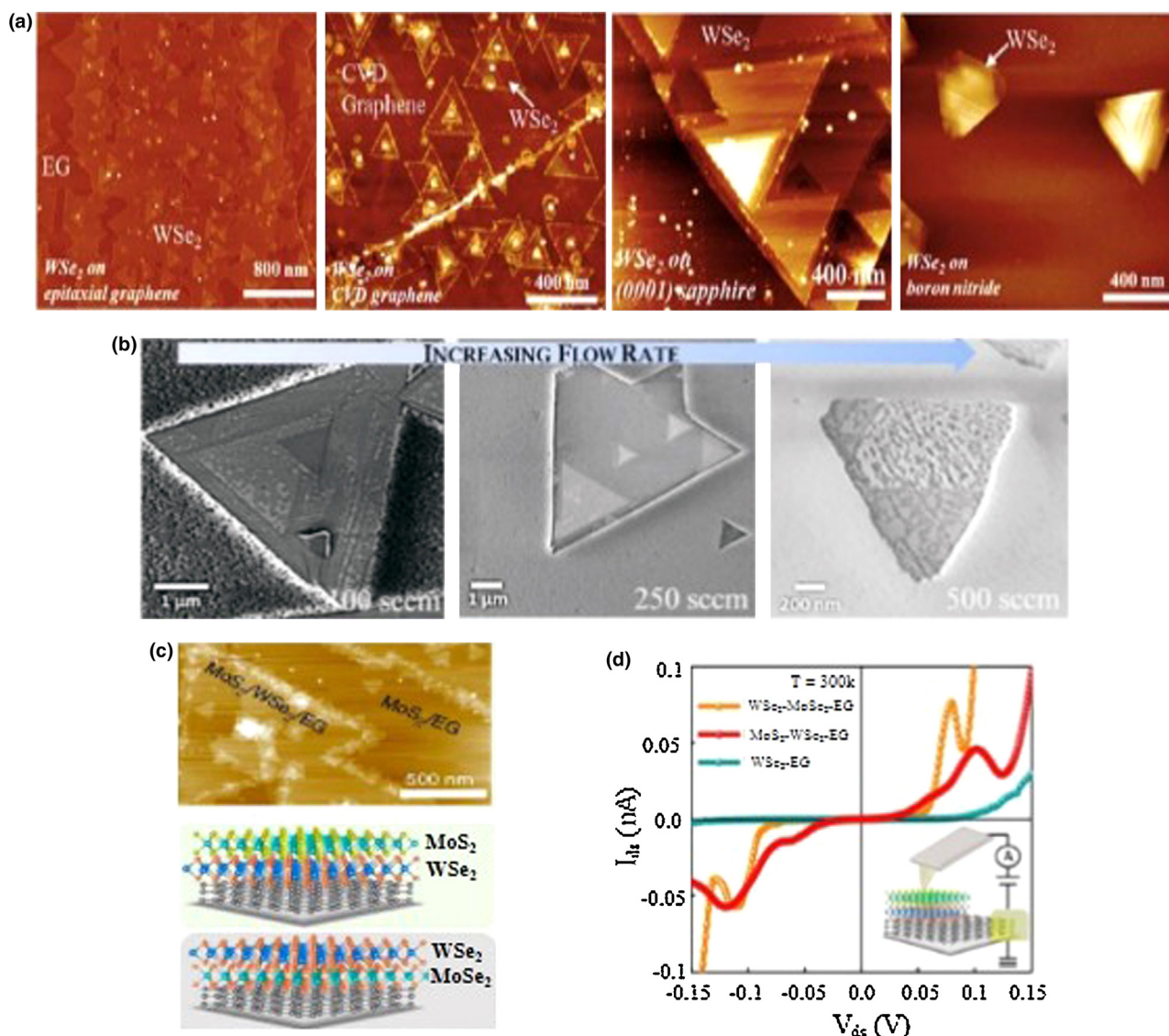
graphene, while the largest domain size of about 5–8 μm was observed on sapphire. Figure 8b shows the influence of the gas flow rate on the domain size and shape of WSe₂ grown on epitaxial graphene. Besides flow rate, the domain size increases with increasing total pressure and temperature. A 200% increment in the grain size (700 nm to 1.5 μm) occurred as temperature rose from 800 to 900°C. The results were similar on sapphire substrates. Besides pressure and temperature, the Se:W ratio and total flow through the system greatly impact the domain size of WSe₂ films. An increase in Se:W ratio from 100 to 2000 allows an increase in the domain size from 1 to 5 μm . An increase in total gas flow from 100 to 250 sccm enhances domain size up to 8 μm . The I-V characteristics confirm the presence of a tunnel barrier to vertical transport created by the WSe₂ and thereby evidences that a pristine van der Waals gap exists in WSe₂/graphene heterostructures. Furthermore, this method is used to grow MoS₂/WSe₂/graphene and WSe₂/MoS₂/graphene heterostructures (Fig. 8c) [97]. Interestingly, they discovered that directly grown heterostructures by MOCVD exhibit resonant tunneling of charge carriers that leads to large negative differential resistance (NDR) at room temperature as shown in Fig. 8d. The MOCVD method is versatile, highly scalable, and provides significant stoichiometric control over the films, but the use of toxic precursors, slow film growth rate and high production cost set it back for the widespread use.

Atomic layer deposition (ALD)

ALD is a gas phase chemical process to deposit atomically thin films of various materials layer by layer by using precursors to react

them with substrate. Although ALD has been used widely for oxide materials, several binary sulfide materials have been studied successfully by several research groups. These include TiS₂, WS₂, MoS₂, tin (II) sulfide (SnS), and lithium sulfide (Li₂S). However, in the scope of the current article, we summarize only important results of the 2D TMDs by ALD method. Tan et al. [98] provided precise control over the MoS₂ film thickness prepared by the self-limiting reactions of molybdenum pentachloride (MoCl₅) and hydrogen sulfide (H₂S) on sapphire substrate. However, high-temperature (800°C) annealing was performed to grow large size (~2 μm) triangular MoS₂ crystals. Song et al. [99] demonstrated the wafer scale growth of WS₂ using the ALD growth of tungsten oxide (WO₃) with subsequent conversion via H₂S annealing. Figure 9a shows the ALD growth steps for the synthesis of WS₂ nanosheets. The number of MoS₂ layers can be controlled effectively by tuning the number of ALD cycles for MoO₃ growth. The camera image of large-area (approximately 13 cm in length) mono-, bi-, and tetralayer WS₂ nanosheets on SiO₂ substrate is shown in Fig. 9b.

Monolayer WS₂ FETs fabricated in the top-gate geometry showed *n*-type conduction with an electron mobility of $\sim 3.9 \text{ cm}^2 \text{ V}^{-1} \text{ s}^{-1}$ (Fig. 9c). Furthermore, the high conformal growth ability of ALD helped them to realize thickness controlled growth of 1D WS₂ nanotubes (WNTs) by sulfurizing WO₃ layers deposited on Si nanowires (NWs). Following the first report on ALD growth of 2D materials, Jin et al. [100] presented another chemical route to deposit MoS₂ on SiO₂/Si substrate using Mo(CO)₆ and dimethylidisulfide (CH₃SSCH₃, DMDS) as Mo and

**FIGURE 8**

(a) AFM surface morphology of the WSe_2 film grown on different substrates; epitaxial graphene, CVD graphene, sapphire, and boron nitride. (b) FESEM images of WSe_2 showing an evolution of domain size as a function of flow rate. (Reprinted with permission from Ref. [96]. 2015, American Chemical Society.) (c) Schematic and AFM image of different heterostructures (d) I - V curves for different combination of dichalcogenide-graphene heterostructures indicating resonant tunneling and NDR. (Reprinted with permission from Ref. [97]. 2013, American Chemical Society.)

S precursors, respectively. The as-deposited sample was annealed at 900°C to crystallize them into a 2H- MoS_2 phase. The above studies reveal clearly that the growth temperature was quite high (800 – 1000°C) and films resulted in crystallite size in sub-10 nm range. Hence, the development of a better ALD approach to grow high quality, large-scale with precise control of atomic layer thickness in MX_2 is imperative. In this direction, Delabie et al. [101] demonstrated the low temperature (300 – 450°C) growth of WS_2 atomic layers enabled by Si and H_2 plasma reducing agents for CVD and ALD, respectively, in the presence of WF_6 and H_2S precursors. No template layer or post deposition annealing treatment was performed on these layers [102]. ALD method is highly scalable with precise thickness controllability usually at low substrate temperatures; its expensive nature and use of highly sensitive precursors are big concerns.

Applications

2D TMD materials are considered attractive for diverse applications including electronics, photonics, sensing, and energy devices. These applications are inspired by the unique properties of layered materials such as thin atomic profile that represents the ideal conditions for maximum electrostatic efficiency, mechanical strength, tunable electronic structure, optical transparency, and sensor sensitivity [103]. Of particular interest for applications is flexible nanotechnology, which is considered for potentially ubiquitous electronics and energy devices that can benefit from the range of outstanding properties afforded by 2D materials. Flexible technology comprises a wide array of scalable large-area devices including thin film transistors (TFTs), displays, sensors, transducers, solar cells and energy storage on mechanically compliant substrates.

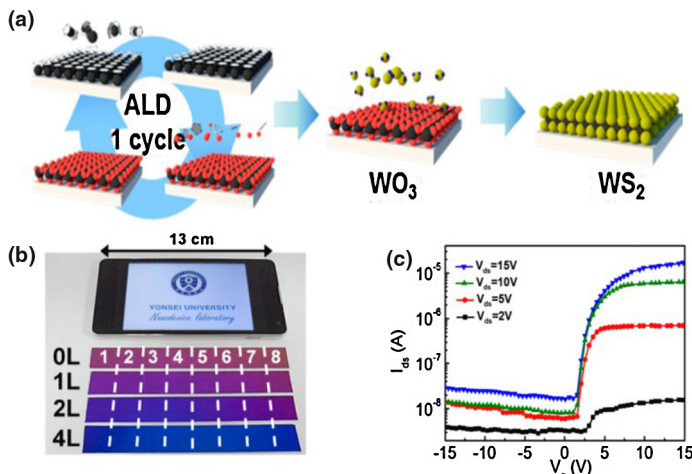


FIGURE 9

(a) Schematic of the ALD process for the synthesis of large area and thickness controlled WS₂ films and (b) demonstration of the large area (approx. 13 cm) mono-, bi-, and tetralayer WS₂ fabricated on Si/SiO₂ substrates. The growth area is about the size of a cellular phone display screen. (c) Transfer characteristics of single layer WS₂ FET exhibiting *n*-type conduction behavior. (Reprinted with permission from Ref. [99]. 2013, American Chemical Society.)

Electrical and optoelectronics applications

The scaling limits of conventional silicon-based technology over the last decades suggest that atomically thin semiconductors such

as TMDs might be applicable for future generation large-scale electronics [104], provided manufacturing and integration challenges can be resolved. Indeed, the first consumer product featuring graphene touch panel displays in smart-phones was released in China in 2014, after only ten years of global graphene research, a relatively short time in the innovation cycle. Moreover, in this timeframe, several articles have reviewed breakthroughs and perceived applications of 2D materials [105,106]. Here, we will discuss progress in flexible electronics, particularly 2D TFTs, which is the core device required for many flexible technology device concepts, much like the conventional ones (FET is the central device for virtually all uses of semiconductor technology).

After several years of active research and development, high-performance 2D TFTs based on synthesized MoS₂ have now been achieved. These TFTs operating at room temperature feature the characteristic high on/off current ratio and current saturation expected from high-quality TMDs (Fig. 10a,b). In particular, electron mobility $\sim 50 \text{ cm}^2 \text{ V}^{-1} \text{ s}^{-1}$ and current density $\sim 250 \mu\text{A}/\mu\text{m}$ have been observed, which is very encouraging for high-performance TFTs. Importantly, cut-off frequencies exceeding 5 GHz have been realized on flexible plastic substrates at a channel length of 0.5 μm (Fig. 10c). At first, this was rather surprising given the relatively low mobility of MoS₂; however, at the high fields needed for maximum high frequency operation, transport is determined by the saturation velocity (v_{sat}) that turns out to be sufficiently reasonable ($\sim 2 \times 10^6 \text{ cm/s}$) to achieve GHz speeds at sub-micron channel lengths [107]. In addition, flexible monolayer MoS₂ TFTs

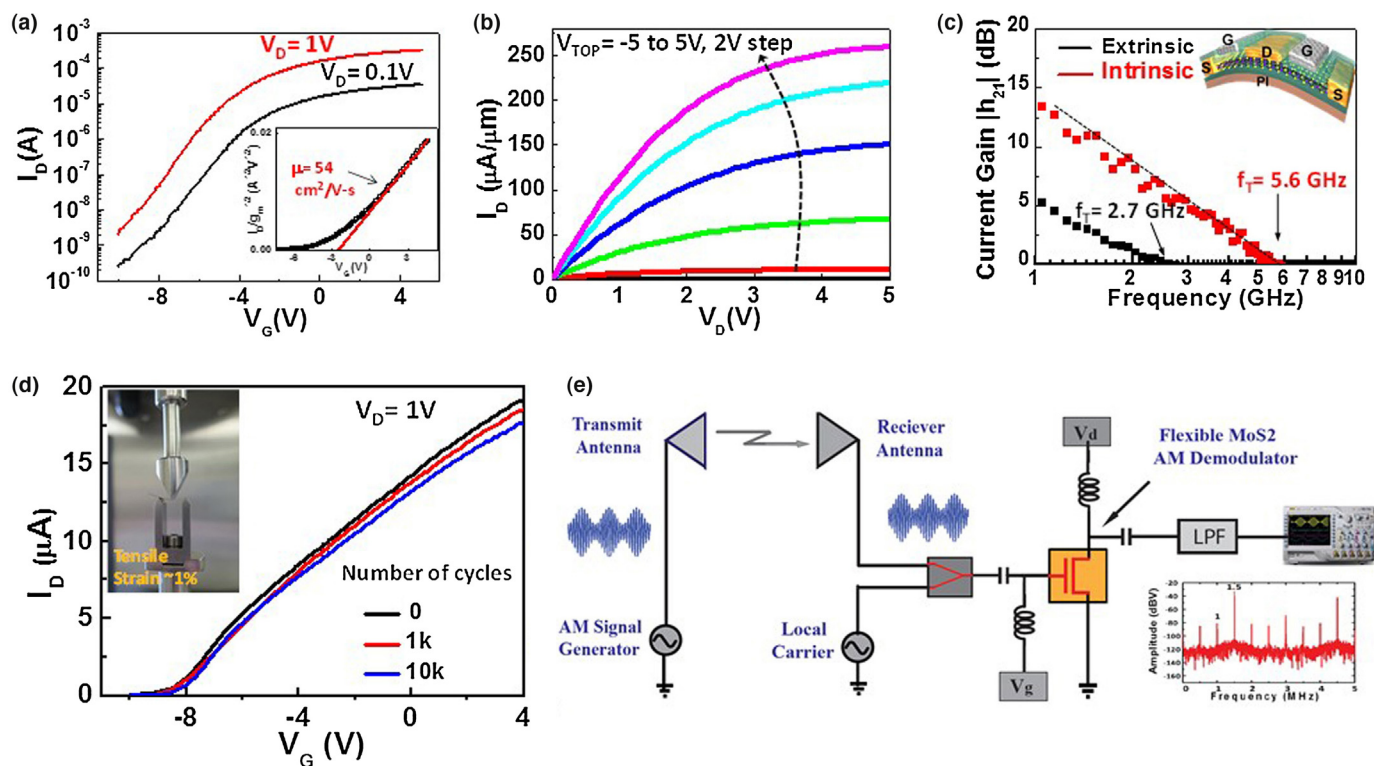


FIGURE 10

Representative CVD-grown MoS₂ FET ($L = 1 \mu\text{m}$, $W = 2.6 \mu\text{m}$) on 280 nm SiO₂/Si. (a) Electrical transfer characteristics. The insert shows the low-field mobility $\sim 54 \text{ cm}^2 \text{ V}^{-1} \text{ s}^{-1}$, which is at the high-end for monolayer MoS₂. (b) I_D - V_D characteristics featuring linear-saturation profile expected for well-behaved semiconducting FETs. (c) Extracted cut-off frequency for flexible MoS₂ transistors with intrinsic $f_T \approx 5.6 \text{ GHz}$ ($L = 0.5 \mu\text{m}$). Inset is an illustration of the device structure. (d) Multi-cycle bending tests showing that the flexible MoS₂ afford strong electrical stability after 10,000 cycles of bending at 1% tensile strain. (e) Schematic of flexible MoS₂ RF transistor used as an AM demodulator within a wireless AM receiver system (AM radio band 0.54–1.6 MHz). Inset shows the AM receiver output spectrum. (Reprinted with permission from Ref. [107]. 2015, John Wiley and Sons.)

offer robust electronic performance to 1000 s of cycles of mechanical bending (Fig. 10d). Altogether, the combined high on/off ratio, saturation velocity and mechanical strength make MoS₂ and related TMDs very attractive for low-power RF TFTs for advanced flexible Internet of Things (IoT) and wearable connected nanosystems. Toward this end, a simple wireless flexible radio receiver system has been demonstrated using monolayer CVD MoS₂ for demodulation of the received signal, the central signal processing function of wireless receivers (Fig. 10e).

For higher speed or frequency operation, newer 2D materials such as BP show significant promise with reported transistor mobility as high as $\sim 1000 \text{ cm}^2 \text{ V}^{-1} \text{ s}^{-1}$ (Fig. 11a), approaching that of CVD graphene, and on/off ratios typically $>10^2\text{--}10^3$ at room temperature [108].

In essence, BP can be viewed as a 2D crystal that offers optoelectronic properties in between zero-bandgap high-mobility graphene and large-bandgap low-mobility TMDs. A primary application of BP is for high-performance high-mobility flexible nano-optoelectronics. In this regard, the first flexible BP TFTs was reported in 2015 [109], and offered ambipolar transport with hole and electron mobilities (Fig. 11b) higher than the established thin-film materials based on metal oxides, organic semiconductors and amorphous Si. This is all the more interesting since the fabricated flexible BP TFTs were not optimized in terms of contacts and interfaces, thereby suggesting significant room for performance improvement. Output characteristics of flexible BP TFTs show strong current saturation (Fig. 11c). The current saturation and

ambipolar properties have been exploited to realize inverting and non-inverting analog amplifiers, and digital inverters and frequency multipliers, respectively, on flexible substrates [110]. Based on the experimental saturation velocity of the different 2D materials from TMDs to graphene, the high-frequency application space for flexible nanosystems is depicted in Fig. 11d. TMDs are suitable for low-power RF and IoT systems, BP with the higher v_{sat} is attractive for wireless microwave and 5G systems, and graphene with the highest mobility and v_{sat} can enable flexible THz detectors and communication systems [111,112].

Energy applications

2D TMDs are gaining significant attention as electrode materials for energy storages, such as supercapacitors and Li-ion batteries, due to their atomically layered structure, high surface area and excellent electrochemical properties. Such layered structures provide more sites for ions in energy storage while maintaining structure stability during charge and discharge cycles. The high surface area of 2D materials (e.g. the surface area of graphene shows $2630 \text{ m}^2/\text{g}$, which is the highest among carbon materials) when combined with surface functionality and electrical conductivity, make them as an ideal electrode for energy storages [113–115].

A supercapacitor is a high-capacity electrochemical capacitor with capacitance values one order higher than Li-ion batteries consisting of two symmetric electrodes separated by a membrane, and an electrolyte ionically connecting both electrodes. When the electrodes are polarized by an applied voltage, ions in the electrolyte form electric double layers of opposite polarity to the electrode's polarity. In certain electrode materials, some ions may permeate the double layer and become specifically adsorbed ions and contribute with pseudocapacitance to the total capacitance of the supercapacitor. MoS₂ exhibits large electrical double layer capacitance (EDLC) due to its stacked-sheet-like structure and large pseudo-capacitance owing to different Mo oxidation states (+2 to +6) and has become a promising supercapacitor electrode material in the 2D materials fraternity [116–118]. However, potential problems associated with its widespread use are small flake size, production with low yield and uncontrollable thickness and defects by the exfoliation and hydrothermal methods [119,120].

Tuning the surface morphology of MoS₂ nanosheets is an important parameter for their superior electrochemical performance. Tour et al. [121] fabricated edge oriented/vertically aligned MoS₂ nanosheets that opened more van der Waals gaps and offered reactive dangling bonds sites to the electrolyte ions and thereby manifest large capacitive properties (Fig. 12a). The sponge-like vertically aligned MoS₂ flexible supercapacitor electrodes demonstrated a high areal capacitance up to 12.5 mF cm^{-2} . The limited electrical conductivity of the most common 2H-MoS₂ phase makes it less attractive material for supercapacitor electrode as reported at instances [122,123]. This compels Rutgers university researchers to develop a metallic MoS₂ phase (1T) which has 10^7 times higher conductance than semiconducting phase (Fig. 12b). The chemically exfoliated MoS₂ nanosheets-derived supercapacitor electrodes demonstrated excellent capacitive performance, with capacitance values ranging from ~ 400 to 700 F cm^{-3} in a variety of aqueous electrolytes [124]. Choudhary et al. [34] reported the direct fabrication of a large-scale and unique

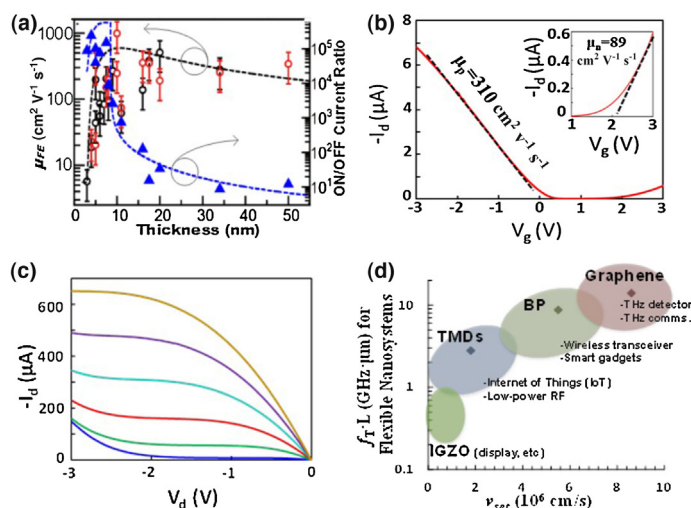
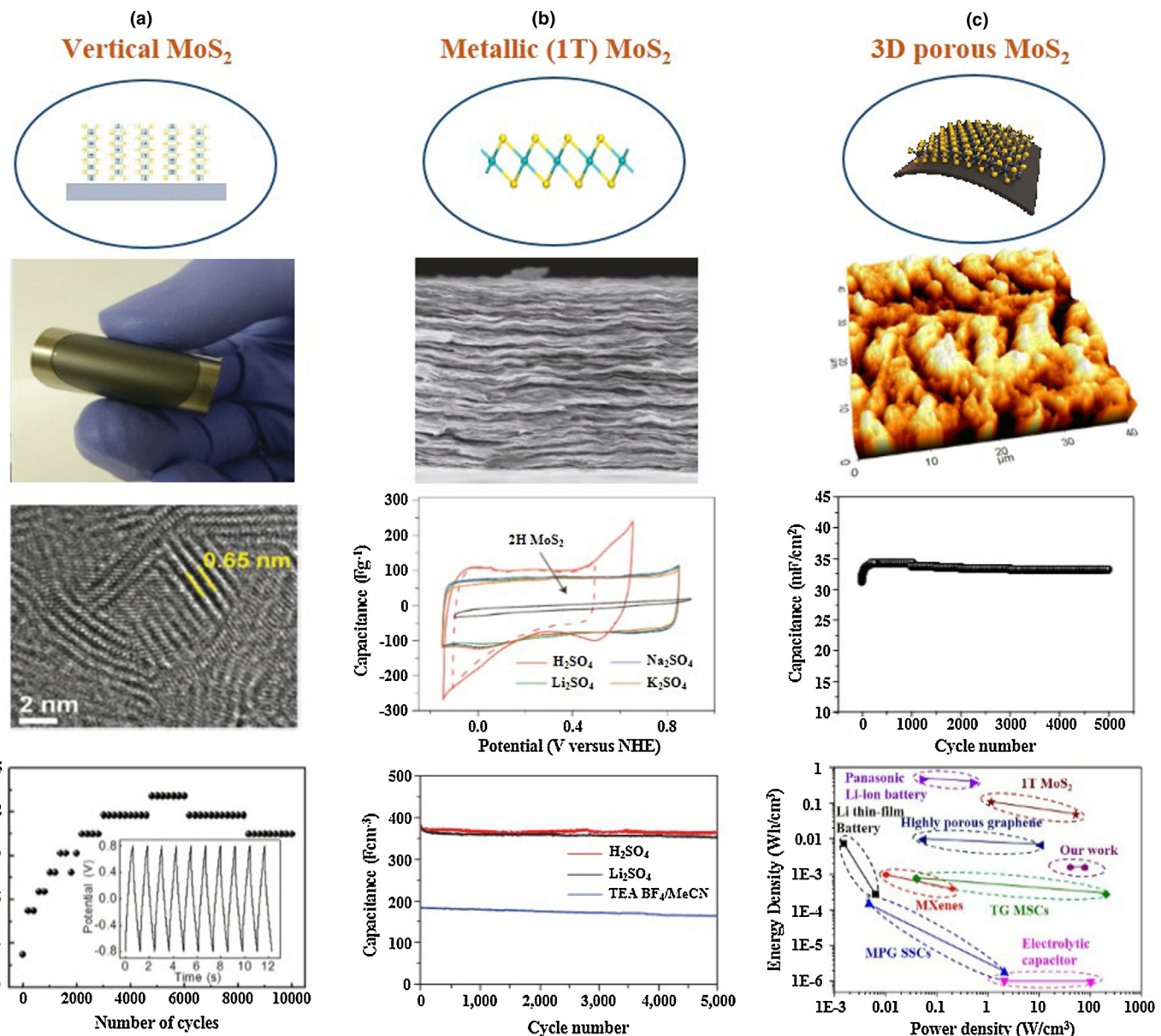


FIGURE 11

(a) Field effect mobility (μ_{FE}) (open circles) $I_{on/off}$ ratio (filled blue triangles) of BP films with varying thickness. (Reprinted with permission from Ref. [108]. 2014, Nature Publishing Group.) (b) Transfer characteristics of encapsulated BP ambipolar TFT on polyimide, showing low field hole mobility of $310 \text{ cm}^2 \text{ V}^{-1} \text{ s}^{-1}$, and electron mobility of $89 \text{ cm}^2 \text{ V}^{-1} \text{ s}^{-1}$. The on/off ratio $>10^3$, $V_d = -10 \text{ mV}$, and flake thickness is 15 nm and $W/L = 10.6 \mu\text{m}/2.7 \mu\text{m}$. (c) Output curves of the same device displaying current saturation. Gate bias, $V_g = 0$ to -2.5 V from bottom to top. (Reprinted with permission from Ref. [109]. 2015, American Chemical Society.) (d) Representative flexible high-frequency nanosystem applications of 2D materials based on experimentally achieved saturation velocities. Contemporary organic and metal-oxide (e.g. IGZO) films are mostly suitable for lower frequency functions such as display TFTs. (Reprinted with permission from Ref. [110]. 2016, American Chemical Society.)

**FIGURE 12**

(a) Flexible MoS₂ electrode, TEM shows the edge-oriented MoS₂ film, and cyclic stability curve showing capacitance retention up to 10,000 cycles. (Reprinted with permission from Ref. [121]. 2014, John Wiley and Sons.) (b) SEM image of chemically exfoliated 1T MoS₂ electrode, CV results of 1T and 2H MoS₂ phase electrochemical performance, and cyclic stability of 1T-MoS₂ electrode. (Reprinted with permission from Ref. [124]. 2015, Nature Publishing Group.) (c) Large scale MoS₂ fabrication on flexible substrates. AFM image shows the 3D-porous MoS₂ structure. (Reprinted with permission from Ref. [34]. 2015, Royal Society of Chemistry.)

3D-porous MoS₂ supercapacitor electrode on flexible substrates (copper, polyimide) using magnetron sputtering techniques, as shown in Fig. 12c. The unique 3D porous surface facilitated the large intercalation of electrolyte ions and exhibited a high areal capacitance of 33 mF cm^{-2} ($\sim 330 \text{ F cm}^{-3}$) at a discharge current density of 25.47 mA/cm^2 . Moreover, the electrode showed $\sim 97\%$ capacitance retention over 5000 cycles, which indicates its excellent cyclic stability. Unlike MoS₂, MXenes are highly conductive and excellent hydrophilic, which allow them to show very large volumetric capacitance of $\sim 900 \text{ F cm}^{-3}$ [125].

Most commercial grade Li-ion batteries are based on graphite anode and lithium cobalt oxide (LiCoO₂) as well as offer

limited theoretical specific capacities of $\sim 670 \text{ mAh/g}$ and measured capacities of 150 mAh/g , which are not suitable to meet the current demand [126,127]. 2D MoS₂ has become an intriguing anode material for Li-ion batteries as it offers a high theoretical capacity of $\sim 670 \text{ mAh/g}$ and large van der Waal gaps between MoS₂ layers that allow the intercalation of Li⁺ ions into the structure without significant volume change and preclude the disintegration of active materials during charging and discharging [128–130]. The electrochemical reaction of Li with MoS₂ involves 4 moles of Li per mole of MoS₂ based on the reaction: $\text{MoS}_2 + 4\text{-Li}^+ + 4\text{e}^- \leftrightarrow 2\text{Li}_2\text{S} + \text{Mo}$, offering ~ 2 times higher storage capacity than that of graphite electrode. In spite of large specific capacity

observed in different MoS₂ morphologies, concerns about its poor cyclic stability and low electronic conductivity have been serious [131,132]. Hence, novel designs of MoS₂-based composite in conjunction with highly conductive nanomaterials like graphene, CNTs could be a solution for the issues. Wang et al. [133] reported high capacity of 400 mAh/g at 0.25 C from the exfoliated MoS₂-C composites. In a recent study, Patel et al. designed and fabricated a hybrid anode material by integrating 3D CNTs with MoS₂ having vertical flake type morphology [134]. The 3D architecture design of CNTs would not only provide the large surface but also facilitate the large amount of loading of the active MoS₂ material. The results reflect an outstanding electrochemical performance with an areal capacity of ~1.65 mAh/cm² (450 mAh/g) at 0.5 C rate, low charge transfer resistance and cycling stability up to 50 cycles at 0.5 C.

Very recently, sodium-ion batteries (SIBs) are being considered to replace lithium-ion batteries (LIBs). However, the large Na⁺ size cannot be accommodated by the graphite anode materials and thereby TMDs such as MoS₂ and WS₂ due to their unique layered structures are considered as highly compatible host anode materials [135]. MXenes have already shown great potential to be used as efficient electrode materials for Li-ion batteries. Mashtalar et al. [136] demonstrated a capacity of 410 mAh/g at 1 C rate on the delaminated Ti₃C₂ based MXene.

2D TMDs sensors

The huge demand for developing highly sensitive, selective, low power consuming, reliable and portable sensors has stimulated extensive research on new sensing materials based on 2D allotropes of TMDs and phosphorous after the great success made by their 2D carbon analog, that is, 'graphene'. The high surface to volume ratio in 2D TMDs offers huge potential for the detection of large amounts of target analysts per unit area as well as rapid response and recovery with low power consumptions [137–139]. Moreover, the recent demonstration of scalable synthesis of 2D TMDs has shown the potential to fabricate cost-effective sensors. Figure 13 shows the use of 2D TMDs such as MoS₂, WS₂, etc. for various sensing applications including gas, chemical, and bio-sensors.

As expected, most of the reported 2D TMDs based sensors have been realized using mechanically exfoliated or liquid phase exfoliated MoS₂ flakes [140,141]. For example, Li et al. [35] fabricated MoS₂-FET sensor device using mechanically exfoliated single and few layer MoS₂ films to detect nitric oxide (NO). It was observed that MoS₂ films exhibited a very high sensitivity to NO with a low detection limit of 0.8 parts per million (ppm). A chemically exfoliated MoS₂ flakes-based sensor by Donarelli et al. [142] outperforms similar sensors, with a measured detection limit of 20 parts per billion (ppb) when exposed to nitrogen dioxide (NO₂) gas. The potential mechanism for the *p*-type behavior of the sensing material (MoS₂) toward NO₂ is the N substitutional doping of S vacancies in the MoS₂ surface. This detection limit is the lowest ever measured to NO₂ for MoS₂-based sensors and is comparable or better than ZnO-, graphene oxide-, and CNT-based sensors. BP and its single atomic layer (phosphorene) have shown great possibility to be effectively employed for gas detection similar to other 2D materials like graphene, MoS₂, etc. [143,144]. Cui et al. [36] reported up to 20 ppb level detection sensitivity in their mechanically exfoliated phosphorene

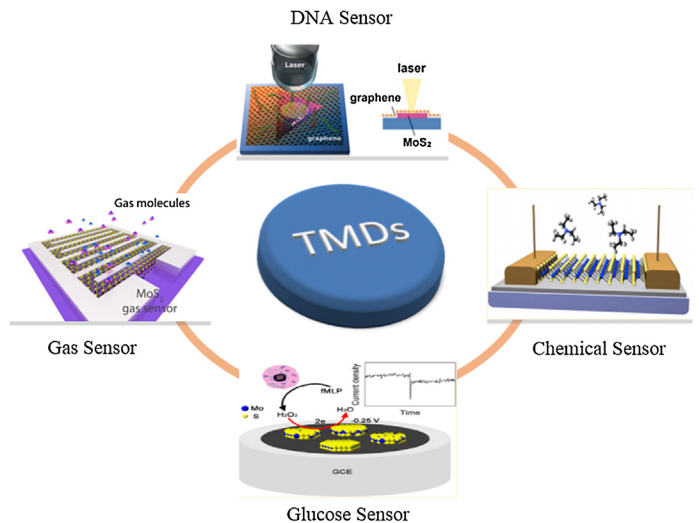


FIGURE 13

Various gas-, chemical- and bio-sensors constructed using 2D TMDs materials like MoS₂, WS₂, etc. (Reprinted with permission from Ref. [146]. 2013, American Chemical Society; Ref. [147]. 2013, American Chemical Society; Ref. [155]. 2014, John Wiley and Sons; Ref. [162]. 2015, Nature Publishing Group.)

nanosheets (PNS)-based FET device in a dry air environment. Abbas et al. [145] reported excellent sensitivity for detection of NO₂ down to 5 ppb using FETs based on few layer phosphorene. Figure 14a,b is the schematic of the multilayer phosphorene FET sensor and its sensing performance at different concentrations of NO₂, respectively. It is observed that phosphorene sensor responds to NO₂ concentrations down to 5 ppb, which is evident by a conductance change of 2.9%. Perkins et al. [146] showed the possibility of using single layer MoS₂ as chemical sensors. The planar FET sensors made with monolayer MoS₂ on Si/SiO₂ wafers showed great response during exposure to various analytes, including standard laboratory chemicals, nerve gas agents, and other solvents like dichlorobenzene, dichloropentane, nitromethane, nitrotoluene, and water vapor.

Biosensing is another important aspect of 2D TMDs that has evidenced significant growth in recent years. Being larger in terms

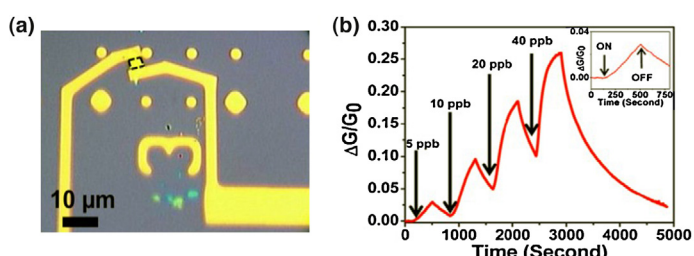


FIGURE 14

(a) An optical image showing multilayer phosphorene FETs using Ti/Au electrodes used for chemical sensing. The thin film flake is bordered by a dashed black line (b) NO₂ gas sensing performance of multilayer phosphorene showing relative conductance change ($\Delta G/G_0$) vs time in seconds for different NO₂ concentrations (5–40 ppb). Inset shows the zoomed image of 5 ppb NO₂ exposure response with identification of points in time where the NO₂ gas is switched on and off. (Reprinted with permission from Ref. [145]. 2015, American Chemical Society.)

TABLE 1

Comparison of the TMDs gas/chemical and bio-sensors with conventional metal oxides and carbonaceous materials-based sensors.

Material	Fabrication method	Gas/chemical tested	Sensitivity	Operating temperature (°C)	Response time
Semiconductor metal oxides					
SnO ₂	Hydrothermal [157]	Ethanol	45.1 ppm	200	Minutes
ZnO	Vapor-phase transport [158]	H ₂ S	17.3 ppm	30	
TiO ₂	Electrospinning [159]	CO	21 ppm	300	
Carbonaceous materials					
CNTs	SWCNT dispersion [160]	NH ₃	3 ppb	R.T.	1–5 s
Graphene	CVD [161]	NO and NO in N ₂	158 ppb	R.T.	
MoS₂	Chemical exfoliation [142]	NO ₂	20 ppb	R.T.	
Phosphorene	Mechanical exfoliation [145]	NO ₂	5 ppb	R.T.	(5–30 s)

of their surface area, 2D TMDs provides the immobilization of large amounts of biomolecules per unit area and can result in high efficiency biosensor leading to excellent detection of biomolecules including DNA, glucose, dopamine, and hydrogen peroxide, just to name a few [147–151]. When compared with the 3D bulk materials and 1D nanomaterials such as silicon nanowires or CNTs based biosensors, 2D TMDs offer high sensitivity and high device scalability as well as high flexibility and transparency. Sarkar et al. [37] demonstrated label free FET-biosensors based on MoS₂ which represents pH detection sensitivity at least 74 times higher compared to graphene based biosensors. There are several reports on efficient DNA detection by MoS₂ based biosensors [152,153]. Farimani et al. [154] demonstrated the efficient DNA base detection using monolayer MoS₂ nanopores. In contrast to graphene nanopore, DNA shows more distinguishable signal per base with 3–5 times less signal to noise ratio in MoS₂ nanopore. However, one of the potential threat to MoS₂-based biosensors for prolong use is their weak immunity to moisture and oxygen that degrades its performance. Chen and co-workers [155] mitigated this problem by making graphene/MoS₂ heterostructures in which graphene serves as a barrier layer between MoS₂ and ambient environment and moreover promotes foreign molecule detection by acting as a host. Similar to MoS₂, WS₂ has been recently reported to show biosensing capability of single-strand DNA (ssDNA) chains via fluorescent quenching [156].

Hence, 2D TMDs (e.g. MoS₂) and phosphorene show the sensitivity up to 20 ppb and 5 ppb, respectively and with the fast response time in the range of 5–30 s. They outperform almost all traditional metal oxides based sensors, which have been limited by long recovery periods and high temperature operations [157–159]. However, the performance/sensitivity of the MoS₂-based FET biosensor has been reported to be 74-fold better than state-of-art 2D graphene-based biosensors. The gas and chemical sensing performance need to be improved to compete with 1D and 2D carbonaceous materials, that is, CNT and graphene [160]. Chen et al. [161] demonstrated that the pristine graphene can detect gas molecule at extremely low concentrations with detection limits as low as 158 parts-per-quadrillion (ppq) with good selectivity. Table 1 is the comparison chart for 2D TMDs and phosphorene gas/chemical sensors with traditional and carbon-based gas sensors.

Despite significant progress, sensors fabricated using mechanical and liquid exfoliation are limited to small-scale fabrication and cannot meet with ever-increasing demand of industrial production. Cho et al. [162] reported more scalable approach by

wafer-scale fabrication of MoS₂ sensor prepared by CVD method whose sensitivity for NO₂ and ammonia (NH₃) was comparable to the exfoliated MoS₂-based sensors [163]. In another study [164], the gas sensitivity of the 2D MoS₂/graphene heterostructure gas sensor can reach a detection limit of about 1.2 ppm to NO₂.

Conclusion and outlook

An in-depth review of recent advances in 2D TMDs materials synthesis and characterization, and their applications are presented. Progress in 2D TMDs materials provides the scientific community with many new opportunities to explore phenomena, concepts and technologies in electronics, opto-electronics and energy. Semiconducting 2D TMDs possess huge potential to be made into ultra-small and low power transistors that are more efficient than state-of-the-art silicon based FETs. With showing the compliance of 2D TMDs materials and flexible substrates, 2D TMDs have attracted considerable interest as flexible devices. Due to their atomically layered structure, high surface area and outstanding electrochemical properties, TMDs have been considered as a candidate for high efficiency energy storages, when combined with surface functionality and electrical conductivity. The large surface-to-volume ratio bestows 2D TMDs-based sensors with improved sensitivity, selectivity and low power consumption. Besides, TMDs have been attracted as new physics called “Valleytronics”, which is due to strong spin-orbit interactions and lack of inversion symmetry at their ultimate atomic thickness. New families of 2D materials, such as BP, silicene, and germanene are expected to open new roads for low dimensional electronic/energy devices, provided their stability issues are resolved.

Despite considerable progress in the synthesis of large-scale and uniform atomic layers of 2D TMDs, the quality of 2D TMDs has not yet reached that of mechanically exfoliated 2D TMDs flakes. To realize practical applications with advanced synthesis methods, key issues that should be advanced include single-layer controllability, defect-less film growth, doping and alloying of TMDs. As advanced synthetic methods currently being developed in the laboratory realize practical applications, we can expect that 2D TMDs whose functions are now only envisioned will revolutionize the electronics, opto-electronics and energy technologies.

Acknowledgements

Y.H.L. acknowledges the support by the Institute for Basic Science (IBS-R011-D1). D.A. acknowledges the support by the Office of Naval Research (ONR) under contract N00014-110190, and the NSF

NASCENT Engineering Research Center (EEC-1160494). W.C. acknowledges the support from the Advanced Materials and Manufacturing Processes Institute (AMMPI) and Research Seed Grants from University of North Texas.

References

- [1] S.Z. Butler, et al. *ACS Nano* 7 (2013) 2898.
- [2] X. Duan, et al. *Chem. Soc. Rev.* 44 (2015) 8859.
- [3] D. Jariwala, et al. *ACS Nano* 8 (2014) 1102.
- [4] S. Mahatha, et al. *J. Phys.: Condens. Matter* 24 (2012) 475504.
- [5] W.S. Hwang, et al. *Appl. Phys. Lett.* 101 (2012) 013107.
- [6] P. Vogt, et al. *Phys. Rev. Lett.* 108 (2012) 155501.
- [7] A. Pakdel, et al. *Mater. Today* 15 (2012) 256.
- [8] Z. Ni, et al. *Nano Lett.* 12 (2011) 113.
- [9] L. Song, et al. *Phys. Rev. B* 86 (2012) 075429.
- [10] L. Ci, et al. *Nat. Mater.* 9 (2010) 430.
- [11] Z. Liu, et al. *Nano Lett.* 11 (2011) 2032.
- [12] H. Zhang, *ACS Nano* 9 (2015) 9451.
- [13] S. Das, et al. *Crit. Rev. Solid State Mater. Sci.* 39 (2014) 231.
- [14] X.-R. Wang, et al. *Chin. Phys. B* 22 (2013) 098505.
- [15] S. Das, et al. *Annu. Rev. Mater. Res.* 45 (2015) 1.
- [16] R. Cheng, et al. *Nat. Commun.* 5 (2014) 5143.
- [17] D. Akinwande, et al. *Nat. Commun.* 5 (2014) 5678.
- [18] W. Bao, et al. *Appl. Phys. Lett.* 102 (2013) 042104.
- [19] G. Frey, et al. *Phys. Rev. B* 57 (1998) 6666.
- [20] M.R. Islam, et al. *Nanoscale* 6 (2014) 10033.
- [21] K.F. Mak, et al. *Phys. Rev. Lett.* 105 (2010) 136805.
- [22] N. Choudhary, et al. *J. Phys.: Condens. Matter* 28 (2016) 364002.
- [23] M.S. Fuhrer, J. Hone, *Nat. Nanotechnol.* 8 (2013) 146.
- [24] N. Choudhary, et al. *J. Mater. Res.* 31 (2016) 824.
- [25] S.S. Varghese, et al. *Electronics* 4 (2015) 651.
- [26] J. Lee, et al. *Sci. Rep.* 4 (2014) 7352.
- [27] N. Perera-Lopez, et al. *2D Mater.* 1 (2014) 011004.
- [28] N. Choudhary, et al. *Sci. Rep.* 6 (2016) 25456.
- [29] A.K. Geim, V. Grigorieva, *Nature* 499 (2013) 419.
- [30] C.-H. Lee, et al. *Nat. Nanotechnol.* 9 (2014) 676.
- [31] K.F. Mak, J. Shan, *Nat. Photonics* 10 (2016) 216.
- [32] S. Lin, et al. *Sci. Rep.* 5 (2015) 15103.
- [33] W. Wu, et al. *Nature* 514 (2014) 470.
- [34] N. Choudhary, et al. *J. Mater. Chem. A* 3 (2015) 24049.
- [35] H. Li, et al. *Small* 8 (2012) 63.
- [36] S. Cui, et al. *Nat. Commun.* 6 (2015) 8632.
- [37] D. Sarkar, et al. *ACS Nano* 8 (2014) 3992.
- [38] G.Z. Madga, et al. *Sci. Rep.* 5 (2015) 14714.
- [39] X. Hong, et al. *Nat. Nanotechnol.* 9 (2014) 682.
- [40] Y. Shi, et al. *Chem. Soc. Rev.* 44 (2015) 2744.
- [41] B. Olofinjana, et al. *J. Mod. Phys.* 2 (2011) 341.
- [42] J.J. Pyeon, et al. *Nanoscale* 8 (2016) 10792.
- [43] H. Oughaddou, et al. *Prog. Surf. Sci.* 90 (2015) 46.
- [44] H. Liu, et al. *ACS Nano* 8 (2014) 4033.
- [45] J. Zhang, et al. *Nano Lett.* 11 (2011) 2407.
- [46] X. Zhou, et al. *J. Am. Chem. Soc.* 137 (2015) 7994.
- [47] D.H. Keum, et al. *Nat. Phys.* 11 (2015) 482.
- [48] M.N. Ali, et al. *Nature* 514 (2014) 205.
- [49] K. Novoselov, et al. *Nature* 438 (2005) 197.
- [50] S.Y. Lee, et al. *ACS Nano* 9 (2015) 9034.
- [51] M.Y. Han, et al. *Phys. Rev. Lett.* 98 (2007) 206805.
- [52] S. Xiao, et al. *Phys. Rev. B* 82 (2010) 041406.
- [53] F. Xia, et al. *Nat. Photonics* 8 (2014) 899.
- [54] O. Del Pozo-Zamudio, et al. *2D Mater.* 2 (2015) 035010.
- [55] S. Tongay, et al. *Nat. Commun.* 5 (2014) 3252.
- [56] C. Ataca, et al. *J. Phys. Chem. C* 116 (2012) 8983.
- [57] R. Kappera, et al. *Nat. Mater.* 13 (2014) 1128.
- [58] Y.-C. Lin, et al. *Nat. Nanotechnol.* 9 (2014) 391.
- [59] R. Kappera, et al. *APL Mater.* 2 (2014) 092516.
- [60] K.-A.N. Duerloo, et al. *Nat. Commun.* 5 (2014) 4214.
- [61] Q.H. Wang, et al. *Nat. Nanotechnol.* 7 (2012) 699.
- [62] S. Das, et al. *Nano Lett.* 13 (2012) 100.
- [63] G.-H. Lee, et al. *ACS Nano* 9 (2015) 7019.
- [64] A. Gastellanos-Gomez, et al. *Adv. Mater.* 24 (2012) 772.
- [65] S. Bertolazzi, et al. *ACS Nano* 5 (2011) 9703.
- [66] J.R. Davis, et al. *ACS Nano* 4 (2010) 6557.
- [67] A.J. Mannix, et al. *Science* 350 (2015) 1513.
- [68] M. Köpf, et al. *J. Cryst. Growth* 405 (2014) 6.
- [69] P. Bridgman, *J. Am. Chem. Soc.* 36 (1914) 1344.
- [70] S. Endo, et al. *Jpn. J. Appl. Phys.* 21 (1982) L482.
- [71] J. Dai, et al. *Wiley Interdiscip. Rev. Comput. Mol. Sci.* (2016).
- [72] D. Hanion, et al. *Nat. Commun.* 6 (2015) 8563.
- [73] D.J. Perello, et al. *Nat. Commun.* 6 (2015) 7809.
- [74] C. Xu, et al. *Nat. Mater.* 14 (2015) 1135.
- [75] Y. Yamada-Takamura, R. Friedlein, *Sci. Technol. Adv. Mater.* 15 (2016) 064404.
- [76] S. Balendhran, et al. *Small* 11 (2015) 640.
- [77] L. Tao, et al. *Nat. Nanotechnol.* 10 (2015) 227.
- [78] X.-Q. Zhang, et al. *Nano Lett.* 15 (2015) 410.
- [79] M.I. Serna, et al. *ACS Nano* 10 (2016) 6054.
- [80] X. Ling, et al. *Nano Lett.* 14 (2014) 464.
- [81] A. Mzerd, et al. *J. Cryst. Growth* 140 (1994) 365.
- [82] R. Waser, *Nanoelectronics and Information Technology*, John Wiley & Sons, 2012.
- [83] Y.H. Lee, et al. *Adv. Mater.* 24 (2012) 2320.
- [84] S. Najmaei, et al. *Nat. Mater.* 12 (2013) 754.
- [85] S. Wang, et al. *Chem. Mater.* 26 (2014) 6371.
- [86] Y. Yu, et al. *Sci. Rep.* 3 (2013) 1866.
- [87] J. Park, et al. *Appl. Phys. Lett.* 106 (2015) 012104.
- [88] Y. Zhan, et al. *Small* 8 (2012) 966.
- [89] G.H. Han, et al. *Nat. Commun.* 6 (2015) 6128.
- [90] A.L. Elias, et al. *ACS Nano* 7 (2013) 5235.
- [91] K.-K. Liu, et al. *Nano Lett.* 12 (2012) 1538.
- [92] Y. Zhang, et al. *ACS Nano* 7 (2013) 8963.
- [93] J. Cheon, et al. *Chem. Mater.* 9 (1997) 1847.
- [94] H.M. Manasevit, *Appl. Phys. Lett.* 12 (1968) 156.
- [95] K. Kang, et al. *Nature* 520 (2015) 656.
- [96] S.M. Eichfeld, et al. *ACS Nano* 9 (2015) 2080.
- [97] Y.-C. Lin, et al. *Nat. Commun.* 6 (2015) 7311.
- [98] L.K. Tan, et al. *Nanoscale* 6 (2014) 10584.
- [99] J.-G. Song, et al. *ACS Nano* 7 (2013) 11333.
- [100] Z. Jin, et al. *Nanoscale* 6 (2014) 14453.
- [101] A. Delabie, et al. *Chem. Commun.* 51 (2015) 15692.
- [102] G. Ham, et al. *ACS Appl. Mater. Interfaces* 5 (2013) 8889.
- [103] J. Kang, et al. *Proc. SPIE* 9083 (2014) 908305.
- [104] G. Fiori, et al. *Nat. Nanotechnol.* 9 (2014) 768.
- [105] G.R. Bhimanapati, et al. *ACS Nano* 9 (2015) 11509.
- [106] A.C. Ferrari, et al. *Nanoscale* 7 (2015) 4598.
- [107] H.Y. Chang, et al. *Adv. Mater.* 28 (2015) 1818.
- [108] L. Li, et al. *Nat. Nanotechnol.* 9 (2014) 372.
- [109] W. Zhu, et al. *Nano Lett.* 15 (2015) 1883.
- [110] W. Zhu, et al. *Nano Lett.* 16 (2016) 2301.
- [111] J.-S. Moon, et al. *2015 IEEE MTT-S International*, 2015, p. 1.
- [112] S. Park, et al. *2015 IEEE International Electron Devices Meeting (IEDM)*, 2015, p. 32.1.1.
- [113] E.G. da Silveira Firmiano, et al. *Adv. Energy Mater.* 4 (2014) 1301380.
- [114] S. Ratha, C.S. Rout, *ACS Appl. Mater. Interfaces* 5 (2013) 11427.
- [115] L. Wang, et al. *RSC Adv.* 5 (2015) 89069.
- [116] X. Fang, et al. *Electrochim. Acta* 81 (2012) 155.
- [117] H. Hwang, et al. *Nano Lett.* 11 (2011) 4826.
- [118] T. Stephenson, et al. *Energy Environ. Sci.* 7 (2014) 209.
- [119] H. Li, et al. *Acc. Chem. Res.* 47 (2014) 1067.
- [120] A.M. van der Zande, et al. *Nat. Mater.* 12 (2013) 554.
- [121] Y. Yang, et al. *Adv. Mater.* 26 (2014) 8163.
- [122] L. Cao, et al. *Small* 9 (2013) 2905.
- [123] J.M. Soon, K.P. Loh, *Electrochem. Solid State Lett.* 10 (2007) A250.
- [124] M. Acerce, et al. *Nat. Nanotechnol.* 10 (2015) 313.
- [125] M. Naguib, et al. *Electrochim. Commun.* 16 (2012) 61.
- [126] V. Etacheri, et al. *Energy Environ. Sci.* 4 (2011) 3243.
- [127] T.-F. Yi, et al. *J. Phys. Chem. Solids* 71 (2010) 1236.
- [128] Y. Shi, et al. *Sci. Rep.* 3 (2013) 1839.
- [129] H. Yoo, et al. *Nanoscale* 7 (2015) 3404.
- [130] J. Zhou, et al. *ACS Nano* 9 (2015) 3837.
- [131] Z. Hu, et al. *Angew. Chem.* 126 (2014) 13008.
- [132] P.P. Wang, et al. *Adv. Mater.* 26 (2014) 964.
- [133] Y.-X. Wang, et al. *Chem. Commun.* 50 (2014) 10730.
- [134] M.D. Patel, et al. *Nanotechnology* (2016).
- [135] X. Xie, et al. *Adv. Funct. Mater.* 25 (2015) 1393.
- [136] O. Mashtalir, et al. *Nat. Commun.* 4 (2013) 1716.
- [137] F. Schedin, et al. *Nat. Mater.* 6 (2007) 652.

- [138] Y. Dan, et al. *Nano Lett.* 9 (2009) 1472.
[139] G. Lu, et al. *ACS Nano* 5 (2011) 1154.
[140] D.J. Late, et al. *ACS Nano* 7 (2013) 4879.
[141] K. K-zadeh, et al. *ACS Sens.* 1 (2016) 5.
[142] M. Donarelli, et al. *Sens. Actuators B: Chem.* 207 (2015) 602.
[143] F. Xia, et al. *Nat. Commun.* 5 (2014) 4458.
[144] L. Kou, et al. *J. Phys. Chem. Lett.* 5 (2014) 2675.
[145] A.N. Abbas, et al. *ACS Nano* 9 (2015) 5618.
[146] F.K. Perkins, et al. *Nano Lett.* 13 (2013) 668.
[147] T. Wang, et al. *Anal. Chem.* 85 (2013) 10289.
[148] T.N. Narayanan, et al. *Nanotechnology* 25 (2014) 335702.
[149] X. Wang, et al. *Biosens. Bioelectron.* 64 (2015) 386.
[150] K. Mao, et al. *Talanta* 132 (2015) 658.
[151] J. Huang, et al. *Electrochim. Acta* 136 (2014) 41.
[152] A.H. Loo, et al. *Nanoscale* 6 (2014) 11971.
[153] R.-M. Kong, et al. *Anal. Bioanal. Chem.* 407 (2015) 369.
[154] A.B. Farimani, et al. *ACS Nano* 8 (2014) 7914.
[155] P.T.K. Loan, et al. *Adv. Mater.* 26 (2014) 4838.
[156] Y. Yuan, et al. *Anal. Chem.* 86 (2014) 3610.
[157] S. Shi, et al. *Sens. Actuators B: Chem.* 140 (2009) 426.
[158] N. Zhang, et al. *J. Appl. Phys.* 103 (2008) 4305.
[159] B. Wang, et al. *Chin. Sci. Bull.* 55 (2010) 228.
[160] F. Rigoni, et al. *Analyst* 138 (2013) 7392.
[161] G. Chen, et al. *Appl. Phys. Lett.* 101 (2012) 053119.
[162] B. Cho, et al. *Sci. Rep.* 5 (2015) 8052.
[163] Q. He, et al. *Small* 8 (2012) 2994.
[164] B. Cho, et al. *ACS Appl. Mater. Interfaces* 7 (2015) 16775.